Monolayer Structure and Evaporation Resistance: A Molecular Dynamics Study of Octadecanol on Water

David J. Henry,[†] Visham I. Dewan,[†] Emma L. Prime,[‡] Greg G. Qiao,[‡] David H. Solomon,[‡] and Irene Yarovsky[†,*]

Applied Physics, School of Applied Sciences, RMIT University, GPO Box 2476 V, Victoria, 3001 Australia, and Department of Chemical and Biomolecular Engineering, The University of Melbourne, Parkville, Victoria, 3010, Australia

Received: October 05, 2009; Revised Manuscript Received: January 11, 2010

This study examines intermolecular interactions of a monolayer of octadecanol ($CH_3(CH_2)_{17}OH$) on water as a function of surface density and temperature, using classical molecular dynamics simulations. We observe increased interaction between the alkyl chains (van der Waals) and hydroxyl groups (H-bonding) with increased surface density, which leads to increased order and packing within the monolayer. We also identified clear trends in the intermolecular interactions, ordering and packing of the monolayer molecules as a function of temperature. The observed trends can be closely related to features of the current empirical theories of evaporation resistance.

1. Introduction

For many years, there has been interest in the effect of monolayers on the rate of molecular transfer across the liquid/gas interface. Molecular monolayers of fatty acids were first demonstrated to be effective at reducing the rate of water evaporation by Rideal[1] in 1925. The evaporation resistance of a monolayer is the additional resistance offered by the monolayer to the overall resistance of movement of water molecules from the liquid to the vapor phase. Subsequently, Langmuir and Schaefer[2] made the first quantitative measurements of the evaporation resistance (r) of monolayers and demonstrated an Arrhenius-type dependence of the resistance of a monolayer to permeation by evaporating water molecules, on temperature.

$$r = C \exp^{\Delta E^{\neq}/RT} \tag{1}$$

where $\Delta E^{\neq}$ is the activation energy for permeation of the monolayer, R is the gas constant, T is the temperature, and C is a constant. This relationship has subsequently been confirmed by a number of other studies with fatty acid monolayers.[3]

Following these early studies, there have been many attempts to use monolayers of simple functionalized alkanes to suppress evaporation from open water bodies.[4−7] Molecular monolayers of long chain alcohols, hexadecanol, and octadecanol were identified as the most promising materials that could reduce evaporative losses by up to 60% from large open water bodies, under suitable conditions. However, the monolayers were easily disrupted by moderate winds. Several experimental studies have also shown that impurities can have a significant effect on the performance of a monolayer.[8,9]

In addition to these applied investigations, there has been considerable effort to develop empirical theories of evaporation resistance based on the experimentally observed trends.[10,11] These include the energy barrier theory,[3,12,13] which is based on the initial Arrhenius-type dependence observed by Langmuir and Schaefer.[2] Barnes and co-workers[3,12] have proposed a modification of eq 1 to explicitly account for the dependence on chain length (n),

$$r = C \exp^{(\Delta G_h^{\neq} + n\Delta G_{CH_2}^{\neq})/RT} \tag{2}$$

where $\Delta G_h^{\neq}$ is the free energy to separate the headgroups and $\Delta G_{CH_2}^{\neq}$ is the free energy to separate CH_2 groups of neighboring alkyl chains. Alternatively, the evaporation resistance can be expanded to incorporate the dependence on surface pressure (Π),

$$\ln r = \ln C' + \Delta E^{\neq}/RT + \Pi \Delta A^{\neq}/RT - \Delta S^{\neq}/R \tag{3}$$

where C' is a constant, $\Delta E^{\neq}$ is the activation energy, $\Delta A^{\neq}$ is the activation area, and $\Delta S^{\neq}$ is the activation entropy. The theory also provides an explanation of the behavior of two-component monolayers in terms of ideal and nonideal mixing; however, it is unable to predict evaporation resistance values or to explain impurity effects.

The density fluctuation theory[14,15] indicates that permeation of the monolayer requires the formation of holes of adequate size and that these holes can be formed from a combination of the available free area in the monolayer and local fluctuation of the surface concentration of monolayer molecules. The theory relates the entropy of expansion (ΔS^e) to the probability (P) of finding a hole of adequate size,

$$P = e^{-\Delta S^e a_w/k_b} \tag{4}$$

where a_w is the area of a water molecule and k_b is the Boltzmann constant. The evaporation resistance is then

$$r = \frac{1}{\alpha}\sqrt{\frac{2\pi M}{RT}}\left(\frac{1}{P} - 1\right) \tag{5}$$

* To whom correspondence should be addressed. E-mail: irene.yarovsky@rmit.edu.au.
† RMIT University
‡ The University of Melbourne

10.1021/jp909544a
Published on Web 03/03/2010

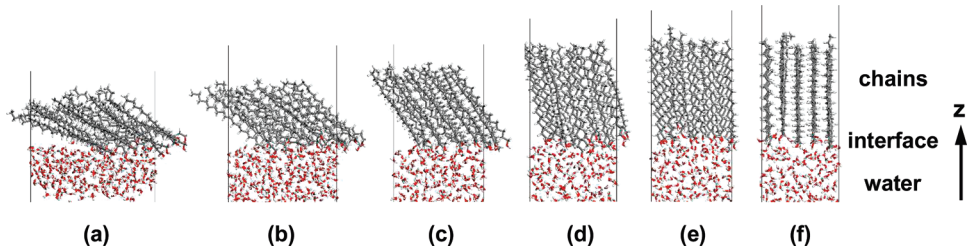

Figure 1. Cross section of typical equilibrium monolayer structure at 298 K and selected surface densities: (a) 45.0, (b) 33.8, (c) 24.2, (d) 20.0, (e) 18.0, and (f) 16.2 Å^2 molecule^{-1}.

where α is the evaporation coefficient and M is the molar mass of water. Barnes and Hunter[10] have found better agreement with experiment if the experimental entropy of spreading is used rather than the entropy of expansion. The density fluctuation theory is able to predict permeation resistance, but there is no explicit allowance for alkyl chain length, and it does not explain impurity effects.

The accessible area theory[4] suggests that evaporation can occur only when there is a naturally occurring hole in the monolayer large enough for the passage of a water molecule, where the total surface area occupied by these holes is the accessible area. Evaporation through the accessible area is assumed to occur at the same rate as through a clean surface. The evaporation resistance is given by

$$r = \frac{1}{\alpha}\sqrt{\frac{2\pi M}{RT}}\left(\frac{A}{a} - 1\right) \tag{6}$$

where A is the total surface area; a is the accessible area; and α, M, and T are the same as for the density fluctuation theory. This model gives reasonable predictions of the evaporation resistance relative to surface concentration of the monolayer. Again, there is no explicit allowance for alkyl chain length or impurity effects, and the results are dependent on the model used to describe the monolayer.

Additional theories include the inhibition of convection, which has been considered by several groups.[16−19] In 1966, Seimiya and Sasaki[20] studied monolayers of stearic acid and cetyl alcohol and proposed that these led to a reduction in the convection current of the water layer due to two factors: first, the suppression of evaporation caused by the monolayer, which reduces temperature differences between the surface and bulk regions of the water; and second, the hydrophilic anchors impart a mechanical resistance to convection of the surface region of the water. However, experimental studies by Barnes and Hunter[19] indicate that monolayers of octadecanol have no effect on the mechanism of heat transfer, so inhibition of convection does not explain the evaporation resistance. X-ray grazing incidence studies[9,21] suggest that the domains of octadecanol are too tightly packed to permit much evaporation and that most evaporation passes through the interdomain regions. These regions are greatly modified by the addition of cholesterol, and this leads to the observed decrease in evaporation resistance.

The molecules of a monolayer can pack in a variety of ways, which leads to a variety of structural phases in the Langmuir monolayer. Each of these phases is generally characterized by an area (Å^2 molecule^{-1}), a surface pressure, and a temperature. Harkins and Copeland[22] first reported the phase diagram for the octadecanol monolayer on water. This phase diagram has subsequently been refined several times with the identification of additional structural phases.[23] Considerable work has also been carried out on studying the properties and transitions between these structural phases.[24−31] Volhardt et al.[32] investigated phase transitions in 2-methyl branched chain alcohols with alkyl chain lengths of C_{10}−C_{18}. They found that the long-range orientational order is strongly reduced in monolayers of 2-methyl alcohols due to less-ordered packing of the alkyl chains in the condensed phase. The packing regime of the monolayer molecules has a significant effect on the level of evaporation resistance.

Simulation studies of simple nonbiological Langmuir monolayers on water include the work of Vysotsky et al.,[33,34] who calculated the thermodynamic functions characteristic of the formation of clusters of alkanols (n = 8−16) at the air/water interface using the PM3 molecular orbital approximation and obtained close agreement with experiment. They found that the aggregation degree of an oligomer increases with alkyl chain length. They also found that entropy factors play a crucial role for the existence of transition states in the formation of clusters and reorganization of the alkanols at the air/water interface. Jang et al.[35] used fully atomistic MD simulations to predict the structure and surface pressure−area isotherms of amphiphilic bistable rotaxane monolayers on the water subphase. Importantly, they found that the isotherms are affected by the unit sequence in rotaxane molecules, a structural feature that determines how the water is incorporated within the monolayer. From these simulations, they were also able to calculate electron density profiles as a function of monolayer packing area, which were in good agreement with experimental values from X-ray reflectometry. Recently, McMullen and Kelty[36] studied the conformational and dynamical properties of monolayers of eicosanoic acid and 18-methyleicosanoic acid using molecular dynamics simulations. They found that the presence of the methyl branch leads to significant changes in the order parameters and film thickness at different surface densities.

The aim of this study is to use classical molecular dynamics to probe the principal intermolecular interactions of a monolayer of 1-octadecanol on water and to identify factors at the molecular level that contribute to water evaporation suppression.

2. Computational Details

Our system is composed of 20 octadecanol ($CH_3(CH_2)_{17}OH$) chains placed over a water layer (Figure 1). The 20 alkanol chains were packed into a 3D periodic cell (30 × 30 × 22 Å) as a nematic liquid crystalline phase using the amorphous cell procedure, which incorporates some features of the original Theodorou−Suter[37] approach and the Meirovitch scanning method.[38] A water layer (20−30 Å) was then added to the cell adjacent to the alkanol layer. The simulation box was then extended to 90.0 Å in the z direction to create a vacuum separation, to prevent interactions occurring across adjacent cells due to 3D periodic boundary conditions imposed on the system. As a result, quasi-2D periodic systems were created.

The COMPASS forcefield[39] has been employed to model the interatomic potentials of the system. The simple point charge

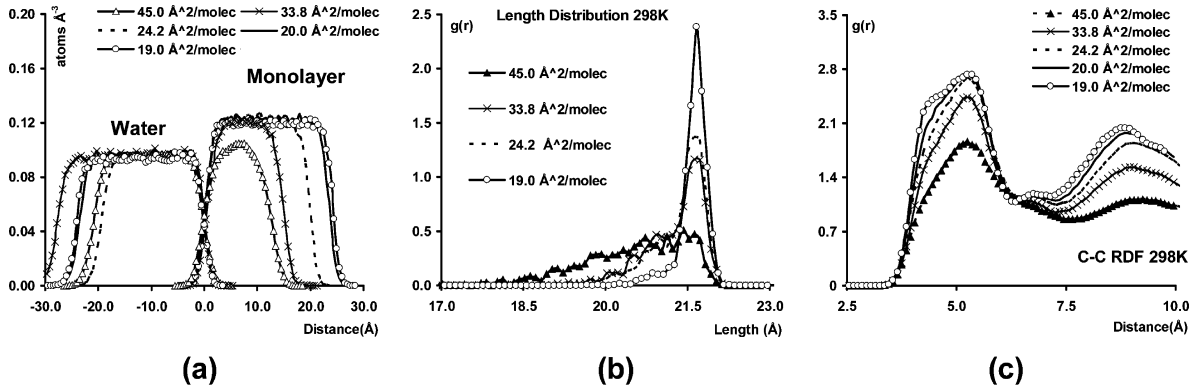

Figure 2. Monolayer properties at 298 K (a), concentration profiles of water and monolayer, (b) alkyl chain length distributions, and (c) intermolecular carbon−carbon radial distribution functions.

(SPC) method was used to model the water molecules.[40] To have a reliable description of the intermolecular interactions, the Ewald method was employed to evaluate all nonbonded van der Waals and Coulomb interactions with an accuracy of 4×10^{-3} kJ mol^{-1}.

To eliminate any potential steric strain produced during the model construction, energy minimization was performed using the conjugate gradient procedure with a convergence limit of 4 kJ mol^{-1} Å^{-1}. Molecular dynamics simulations were performed in the NVT ensemble, equilibrated for 1 ns with data acquisition for 1 ns, using a 1.0 fs time step. The temperature was maintained at 298 K with the Anderson thermostat[41] with a collision ratio of 1.0.

In a typical experiment, the monolayer material is spread across the surface of the water in a Langmuir trough and then gradually compressed. We have simulated this process by initially starting with a system of 20 chains contained in a periodic cell with dimensions $30 \times 30 \times 90$ Å (surface density = 45.0 Å^2 molecule^{-1}), which represents a low-surface-density monolayer. Molecular dynamics was run for at least 1 ns to equilibrate the system, and then data were acquired for 1 ns. Following this, the system was compressed in the x and y dimensions by 2.0 Å and re-equilibrated (1−10 ns), and then data were acquired at the new surface density for 1 ns. This compression process was repeated in 2.0 Å steps until a cell size of $20 \times 20 \times 90$ Å was reached (surface density = 20.0 Å^2 molecule^{-1}) and then in 0.5 Å steps until the monolayer was observed to form a 2D solidlike phase or monolayer collapse was observed ($18.0 \times 18.0 \times 90$ Å, surface density = 16.2 Å^2 molecule^{-1}). The compression process was performed at 273, 288, 298, 308, 318, and 368 K. In the following discussion, a low surface density corresponds to a high area per molecule. Similarly, a high surface density corresponds to a low area per molecule.

The local organization of the hydrogen bonding network of water was described by calculating values of the total number of hydrogen bonds (H-bonds) per water molecule. This was calculated as the average over the final 250 ps of the equilibrium trajectory. A hydrogen bond criterion was defined by a cutoff distance of 2.5 Å and a donor−hydrogen−acceptor cutoff angle of 90°.[42] Specific interactions between the atoms of the monolayer and the water were characterized by averaging the radial distribution function $g(r)$ over the final 1 ns of the trajectory. Values of $g(r)$ were normalized to account for the vacuum spacer introduced in the cell to mimic a 2D interface. The $g(r)$ for carbon to carbon is determined solely as the intermolecular component and, therefore, excludes contributions between bonded carbons within the same chain. The average maximum thickness of the alkyl chain region can be determined by monitoring the distance, in the z direction, between the highest and lowest carbon atoms during the simulation. The free volume of the monolayer was determined as the volume remaining after removal of the water layer, the vacuum spacer, and the volume occupied by the van der Waals surface of the monolayer. Tilt angle was calculated as the angle between the plane of best fit for a row of chains of the monolayer and the z axis of the cell, averaged over the final 250 ps.

3. Results and Discussion

A. Monolayer Structure and Properties at 298 K. Simulations were started with the hydroxyl groups located close (1−2 Å) to the water interface and the alkyl chains generally well-ordered. Figure 1 displays cross sections of the monolayer at 298 K for surface densities from 45.0 to 16.2 Å^2 molecule^{-1}, which demonstrate the progression of the monolayer structure from low to high surface densities (≈ high surface pressures). At the lowest surface density (45.0 Å^2 molecule^{-1}) there is relatively little structural order; however, as the surface density is increased, there is an increase in order and a decrease in the tilt of the molecules until a transition to a solidlike 2D phase (Figure 1f) is reached. The transition to a solidlike phase is demonstrated by a shift to a sawtooth profile in the concentration profile of the monolayer with periodicity of ∼3.5 and ∼1.0 Å in the x and z directions, respectively, indicating a regular crystal type packing of the chains that does not change during the course of the simulation. Similarly, the intermolecular carbon−carbon radial distribution function exhibits three peaks spaced by 0.65 Å. Our simulations indicate that at 298 K, the octadecanol monolayer solidifies at surface areas below 19.0 Å^2 molecule^{-1}, and we define the minimum area (maximum density) at this point.[43]

In this section, we will focus on the monolayer properties at 298 K for surface densities from 45.0 (low surface pressure) through to 19.0 Å^2 molecule^{-1} (high surface pressure region).[22,23] The low-surface-density (low-pressure) monolayer phases are generally not associated with evaporation resistance; however, identification of the evolution of the monolayer structure at the atomistic level and the trends in intermolecular interactions provides valuable understanding of the origin of the key interactions.

Figure 2a demonstrates how the concentration profile of our system changes as the surface density (pressure) increases. At 45.0 Å^2 molecule^{-1}, the hydrophobic chains are highly disordered, tending to intertwine and lie across the surface of the water (Figure 1a). This is evident in the concentration profile by a narrow band with fluctuating density across the monolayer

region. As the cell is compressed, the chains become more ordered; consequently, the chains extend farther in the z direction, leading to a broader peak, and there is an increase in the atomic density of the layer. At the highest surface density, the concentration profile of the monolayer plateaus, remaining almost constant across the extent of the monolayer, reflecting uniform packing.

The average maximum thickness of the monolayer in the low-density region (45 Å^2 molecule^{-1}) is 16.3 Å. As the surface density increases, the chains pack together more tightly with increasing structural order, which leads to a much thicker layer of ∼25.5 Å at a surface density of 19.0 Å^2 molecule^{-1}. The full length of the carbon chain for the all-trans conformation of an octadecanol molecule is 21.7 Å. It should be noted that the average maximum thickness of the alkyl layer for surface densities from 19.0 to 20.0 Å^2 molecule^{-1} is larger than the length of a fully extended octadecane chain. This arises from one or more chains being displaced in the z direction such that the head or tail of the molecules extend into the water or vacuum space, respectively.

It is clear from Figure 1 that there are changes in the tilt angle of the monolayer molecules as the system is compressed. At 298 K and a surface density of 45.0 Å^2 molecule^{-1}, the alkyl chains of the monolayer exhibit a tilt of ∼50°. The tilt angle decreases gradually (∼50 to 34°) as the system is compressed to 24.2 Å^2 molecule^{-1}. From this point onward, the tilt angle decreases more rapidly with increasing surface density, reaching a value of ∼2° at a surface density of 18.0 Å^2 molecule^{-1}. The continuous decrease in tilt angle observed in our calculations up to the transition region is in agreement with the experimental plots of Lautz and co-workers,[25,27] although our values are generally slightly smaller than the experimental values. However, since our calculations are performed within the NVT ensemble and, hence, have a fixed cell geometry (cubic), we are unable to characterize the transition to the untilted distorted hexagonal phase and the crystalline herringbone solid phase. For these untilted structures, the barrier length of the monolayer is very close to the length of the alkyl chain, and the shortest path for evaporation of a water molecule corresponds to the formation of a channel between the octadecanol molecules.

Figure 2b displays the length distribution for the alkyl chains at selected surface densities. At the lowest surface density, the monolayer molecules are generally not fully extended due to the presence of kinks in the chains; consequently, the length distribution extends from ∼18.5 to 22.0 Å without any clearly defined peaks. As the surface density is increased, there is an increase in intensity between 20 and 22 Å, with the appearance of a significant peak at 21.7 Å. For surface areas less than 33.8 Å^2 molecule^{-1}, there is essentially no change in the length distribution profile, with a single intense peak at 21.7 Å and a slight shoulder from ∼20 to 21.2 Å. The peak at 21.7 Å is indicative of the all-trans conformation, which enables the highest packing density of the hydrophobic chains in the monolayer. The presence of the small shoulder at slightly shorter lengths indicates the occurrence of small fluctuations in the chain structure at 298 K due to transient local gauche conformations. These results compare favorably with the external infrared reflection-adsorption spectroscopy study of Gericke et al.,[44] who note that there is only a slight shift in the antisymmetric stretching vibration of the closely related 1-hexadecanol during monolayer compression (32−19.5 Å^2 molecule^{-1}), indicating that the chains of the molecules are well-ordered, even in the liquid condensed/gaseous coexistence region.

By monitoring the internal structure of the monolayer, we can also obtain a better understanding of the important intermolecular interactions. The intermolecular radial distribution function (RDF) between carbon atoms provides a measure of the average separation between the alkyl chains. At all surface densities up to 19.0 Å^2 molecule^{-1}, we observe a broad peak at ∼5.3 Å (Figure 2c). This distance is significantly larger than the nonbonded equilibrium separation between alkyl type carbons (∼3.86 Å) and demonstrates that the intermolecular interactions between the alkyl chains are dominated by next nearest neighbors (NNN), in agreement with experimental studies of tilted phases.[30] Therefore, the energy ($\Delta H^{\neq}_{CH_2}$) and entropy ($\Delta S^{\neq}_{CH_2}$) to separate neighboring chains should be low, making $\Delta G^{\neq}_{CH_2}$ low. This contributes to the low evaporation resistance of these monolayer structures. The broadness of the distribution also reflects the high degree of disorder in this phase of the monolayer. As the system is compressed, the carbon−carbon RDF exhibits a shift in the $g(r)$ distribution to shorter distances, and eventually at the higher surface densities, a shoulder develops at 4.25 Å. This indicates a stronger van der Waals interaction between the carbon atoms of the respective nearest neighbor alkyl chains and, therefore, should lead to an increase in the activation energy to separate the alkyl chains ($\Delta H^{\neq}_{CH_2}$).

To further characterize the monolayer structure, we have analyzed dihedral distributions for different regions of the chains (Figure 3). Gericke et al.[44] found that the collective tilting of the film molecules can respond to a change in area more quickly than a reduction in the number of gauche conformers. In this regard, their results show that in general, the middle part of the alkyl chain is the most ordered region of the monolayer. If the headgroup is smaller than any of the other groups along the amphiphilic chain, the headgroup region of the chain tends to be less ordered than the tail end region.

We find that even at the lowest surface density, the dihedral angle for the tail ($C^{15}-C^{16}-C^{17}-C^{18}$) region is largely populated in the trans conformation but that there is a significant population (∼20%) in the gauche conformation. At an intermediate surface density (24.2 Å^2 molecule^{-1}), there is a decrease in the gauche conformations (∼14%), and by the time the system has been compressed to a surface density of 19.0 Å^2 molecule^{-1}, the gauche conformations for the tail region (∼2%) have largely been eliminated. In comparison, for the central region ($C^8-C^9-C^{10}-C^{11}$) of the alkyl chain, we see that there is very little population for the gauche conformations (∼5%) at 45 Å^2 molecule^{-1} and that for the higher surface densities, these have been completely eliminated. Therefore, the activation entropy for separation of the chains ($\Delta S^{\neq}_{CH_2}$) should show a large increase as the system is compressed.

For the headgroup region ($O^1-C^1-C^2-C^3$) of the alkanols (Figure 3b), we see that at low surface density, there are very similar populations for trans and each of the gauche conformations. This indicates that there is significant disorder in the headgroup region; therefore, the activation entropy for separation of the head groups ($\Delta S^{\neq}_{h}$) will be small. As the system is compressed, there is relatively little change in population of these three conformations until a surface density of 24.2 Å^2 molecule^{-1} is reached, at which point the trans conformation begins to exceed either of the gauche conformations. When the system has reached a surface density of 19.0 Å^2 molecule^{-1}, the trans conformation is clearly dominant; however, the gauche conformations still retain nonnegligible populations (∼35%). Consequently, there will be a small increase in $\Delta S^{\neq}_{h}$ with compression. Collazo et al.[45] postulate that both the tilt and the conformational order are closely related to the sterical demand

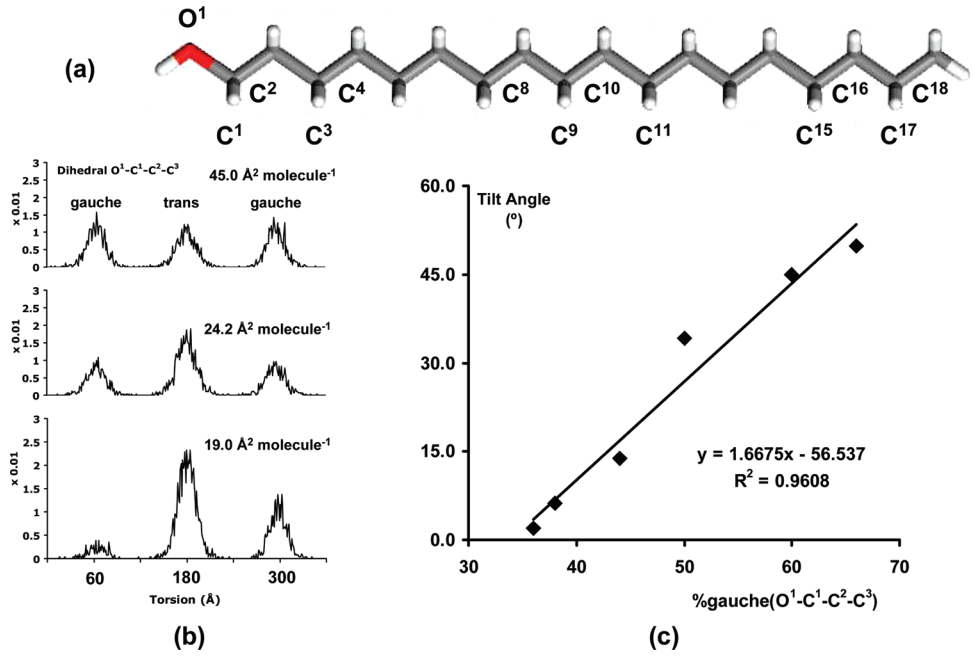

Figure 3. (a) Schematic of octadecanol with key atoms labeled. (b) Dihedral distributions for headgroup ($O^1-C^1-C^2-C^3$). (c) Plot of average tilt angle versus percentage population of gauche conformation in the headgroup ($O^1-C^1-C^2-C^3$).

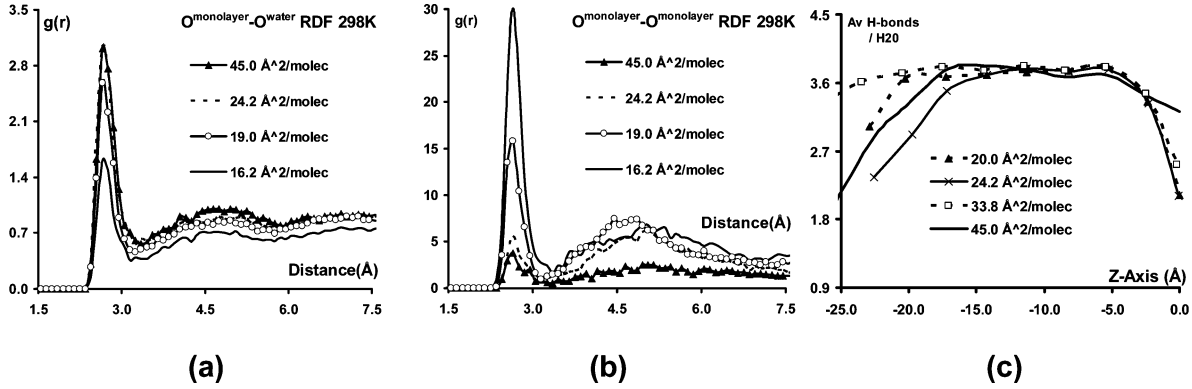

Figure 4. (a) Monolayer oxygen-to-water oxygen RDF. (b) Intermolecular monolayer oxygen-to-monolayer oxygen RDF. (c) Hydrogen bonding as a function of water depth from monolayer interface.

of the headgroup. In Figure 3c, we plot tilt angle as a function of the percentage of gauche conformations for the headgroup dihedral ($O^1-C^1-C^2-C^3$). In agreement with the postulate of Collazo, we see a strong correlation between the tilt angle of the monolayer and the conformation of the headgroup.

At all densities, we see that the hydrophilic hydroxyl groups anchor in the surface region of the water. The specific interaction of the hydrophilic OH groups with the water is demonstrated by the intermolecular radial distribution functions between water oxygen atoms and the alcohol oxygen atoms of the alkanols. Figure 4a reveals that there is a decrease in the first peak of the RDF for monolayer oxygen to water oxygen ($O^{monolayer}-O^{water}$) as the monolayer surface density is increased. This indicates that there is a decrease in the degree of hydrogen bonding between the hydrophilic headgroups of the monolayer and the water.

In contrast, we note that in Figure 4b, there is a very significant increase in the peak intensity for intermolecular oxygen interactions ($O^{monolayer}-O^{monolayer}$) of the alkanol chains with increasing monolayer surface density, indicating that there is increased H-bonding between the neighboring head groups of the alkyl chains. This may explain the slight decrease in the alkanol H-bonding with water at the interface. The existence of specific interaction between head groups at low surface areas per molecule (high surface densities) provides evidence for the importance of including the free energy of activation for separating head groups ($\Delta G_h^{\neq}$) in the energy barrier theory[12] of evaporation resistance (eq 2).

These results also agree with the investigation of Ma and Allen[46] on the conformation and hydration of monolayers composed of closely related lipid components of lung surfactants at the air−water interface. Using sum frequency generation spectroscopy, a surface-selective vibrational spectroscopic technique, they were able to demonstrate how water is squeezed out from the hydration shell of the headgroup during compression of the monolayer, leaving a less hydrated headgroup to anchor the lipid at the air−water interface. A decrease in the hydration of the headgroups of the octadecanol molecules means a decrease in the anchoring to water, which in turn can lead to poor stability with regard to volatilization and wind.[10] This demonstrates the importance of finding and maintaining the optimal surface density for evaporation resistance.

The intermolecular $O^{water}-O^{water}$ radial distribution functions reveal essentially no change with the increase in monolayer surface density because they are dominated by bulk water structure. Figure 4c displays the water-to-water H-bonding

density at 298 K as a function of water depth for selected monolayer surface densities. The major difference between the profiles is the extent over which bulklike behavior is observed due to the compression of the cell ($x-y$ direction) and therefore expansion of the water layer in the negative z direction. All the profiles show an average of 3.6 H-bonds per water molecule in the bulk region, which indicates that there are no significant changes in the structuring of water with the compression of the octadecanol monolayer. However, close inspection of the interfacial region reveals some differences as a function of surface density. In particular, we notice that the H-bonding density at the interface decreases as the monolayer surface density increases. This is in agreement with the O−O radial distribution functions that revealed a significant increase in $O^{monolayer}-O^{monolayer}$ interactions with increasing surface density with a corresponding slight decrease in $O^{monolayer}-O^{water}$ interactions.

Schwendel et al.[47] used neutron reflectivity measurements to probe the density of water at the interface with a self-assembled monolayer. For hydrophilic-terminated undecylthiolate monolayers, they found only a minor deviation in the density of water in the interphase region from that of bulk water. However, as the hydrophilicity of the terminal group is reduced, they found an extended density-reduced water layer next to the monolayer. For the hydrophobic octadecanthiol monolayer, they found the effect was further extended with a very low density water layer adjacent to the monolayer, followed by a second layer with slightly reduced density as compared with bulk. We see in our 20.0 Å^2 molecule^{-1} system that the water-to-water H-bond density at the edge of the interface is ∼57% that for the bulk water region. However, within 2 Å, this has already reached 90% of the bulk water value, and within 5 Å, we observe the bulk water H-bonding density.

At low surface density, there is a very large free volume, equivalent to the volume of ∼15.5 water molecules per octadecanol chain. This provides minimal impedance to a permeating water molecule and, hence, makes a significant contribution to the low evaporation resistance of these structures. As the system is compressed and the chains pack more closely together, the free volume steadily decreases, reaching a minimum equivalent to <6 water molecules per octadecanol chain at a surface density of 19.0 Å^2 molecule^{-1}.

Equation 2 relates the evaporation resistance to the length of the chains and the free energy required to separate CH_2 groups of neighboring alkyl chains. In a strict sense, this relation is only relevant at high surface pressures, but an important observation is that the evaporation resistance is dependent on the effective barrier length that the permeant molecule must traverse to evaporate. At very low surface densities (45.0 Å^2 molecule^{-1}), the chains are tilted and not fully extended. Consequently, the alkyl layer thickness is greatly reduced, providing a much smaller effective barrier length than would be predicted for $n = 18$. At slightly higher surface densities (∼24−34 Å^2 molecule^{-1}), we observe that the alkyl chains are generally fully extended; however, the chains still exhibit significant tilt such that the effective alkyl layer thickness remains less than 20.0 Å. Below ∼24 Å^2 molecule^{-1}, the chains are fully extended and the tilt angle is relatively small, creating the maximum barrier for water evaporation. These observations raise the question about the exact pathway that the water molecules follow during evaporation. Do the water molecules move more or less perpendicularly to the plane of the water/monolayer interface or alternatively, do they follow a path down channels parallel to the aligned alkyl chains that can be tilted? In the first case, the effective barrier is only close to nCH_2 for a relatively untilted monolayer; however, in the second case, the effective barrier length is always nCH_2, for any well-ordered monolayer, regardless of tilt. In the time frame of the present simulations, we do not observe any evaporation of water molecules. Future work will attempt to directly address this question.

B. Effect of Temperature on Monolayer Structure. The Arrhenius-type dependence of evaporation resistance on temperature (eqs 1 and 2) indicates that the evaporation resistance should decrease with increasing temperature; however, understanding the effects of temperature on the structure evolution of the monolayer can provide valuable insight into the origins of the key contributions leading to effective evaporation resistance. We have carried out simulations of the monolayer structure at a range of temperatures from quite a low value (273 K) through to quite a high value (368 K). From these simulations, we have observed that there are subtle trends in the properties and structure of the monolayer within the expected application range of monolayers (288−318 K); however, the general features are quite similar to those already discussed in part A (298 K). Therefore, to clearly highlight the effects of temperature on the structure and characteristics of the monolayer, we will focus in this section on each of the properties considered in Part A, at both low (273 K) and high temperatures (368 K).

At low temperature (273 K), the monolayer is generally slightly more condensed, but the maximum packing density remains, ∼19 Å^2 molecule^{-1}. In comparison, at 368 K, the maximum packing density is between 19 and 20 Å^2 molecule^{-1}; however, at higher surface densities (16.2 and 17.0 Å^2 molecule^{-1}), we observe monolayer collapse rather than the formation of a 2D solid phase. The concentration profile for the monolayer/water system at low temperature (273 K) (Figure 5a) is generally very similar to that observed at 298 K, but the transition to the maximum (plateau atomic density) occurs earlier (i.e., at lower surface density) than was observed at 298 K. In comparison, at 368 K (Figure 5b), the maximum atomic density is observed only at a monolayer surface density of 19.0 Å^2 molecule^{-1}, reflecting the greater structural disorder throughout the system due to the increased kinetic energy.

Figure 5c displays the average maximum thickness of the monolayers as a function of temperature and surface density. At 273 K, we observe the same increase in alkyl layer thickness with compression that was observed at 298 K; however, the values are generally slightly smaller, converging only at a surface density of 18.0 Å^2 molecule^{-1}. In comparison, the average maximum thickness at 368 K generally remains larger than at 298 K for all surface densities, but the difference decreases between 20 and 24 Å^2 molecule^{-1}, before increasing again near the maximum packing density, where it reaches ∼30 Å. These results reflect the high level of chain displacement and disorder that creates free space within the layer at high temperature and, hence, would lead to an overall decrease in evaporation resistance.

Figure 6a displays the average tilt angle of monolayer molecules as a function of surface area at 273, 298, and 368 K. As noted earlier, the tilt angle of the molecules decreases with compression of the monolayer, in agreement with experiment. Interestingly, at 273 K, the average tilt angle shows a steady linear decrease in magnitude with compression down to 20 Å^2 molecule^{-1}, followed by a rapid decrease as the maximum packing density is approached. At 368 K, the monolayer initially

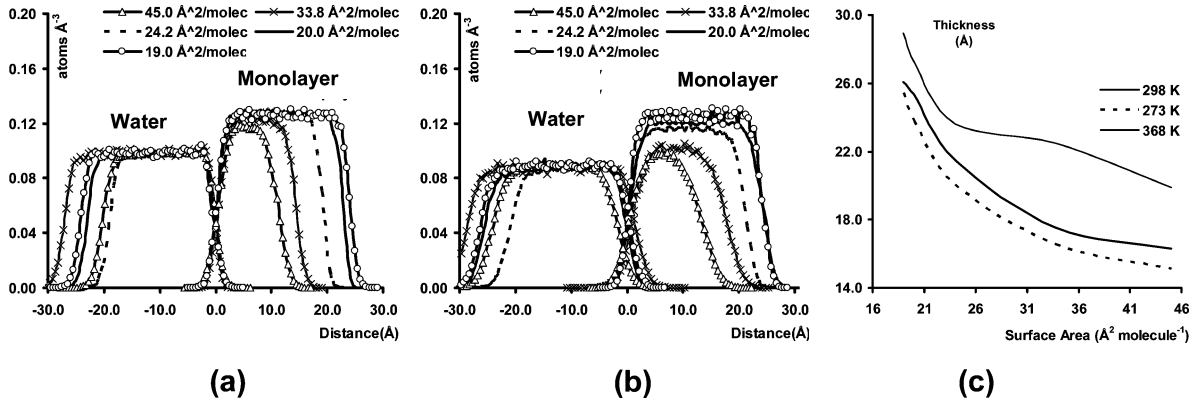

Figure 5. (a) Concentration profiles of water and monolayer at 273 K. (b) Concentration profiles of water and monolayer at 368 K. (c) Average maximum alkyl layer thickness, as a function of temperature and surface density.

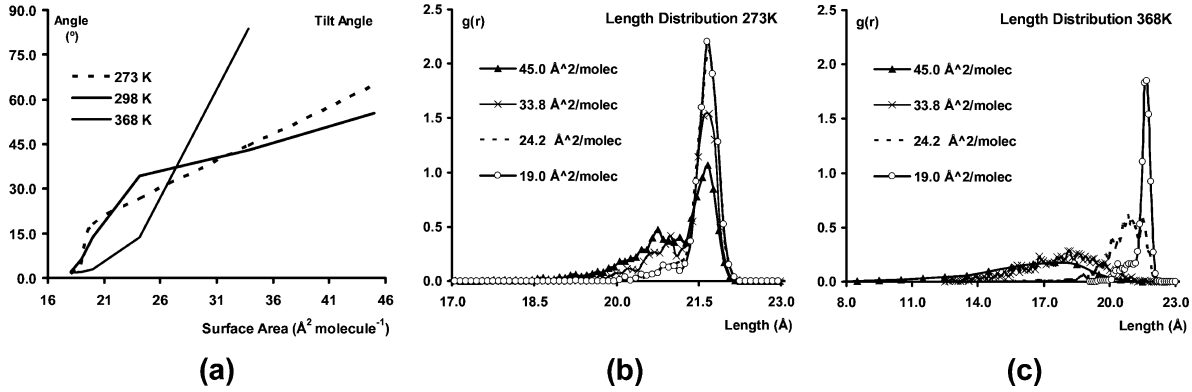

Figure 6. (a) Alkyl chain tilt angle, (b) alkyl chain length distribution at 273 K, and (c) alkyl chain length distribution at 368 K.

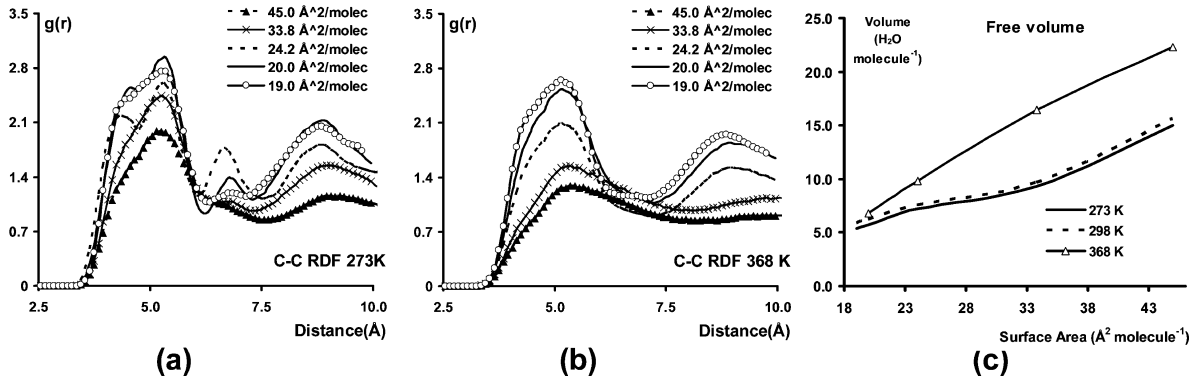

Figure 7. (a) Carbon−carbon radial distribution functions at 273 K, (b) carbon−carbon radial distribution functions at 368, and (c) free volume as a function of surface density at 273, 298 and 368 K.

adopts an extremely titled conformation, but the tilt angle decreases much more rapidly with compression than at 273 and 298 K.

Figure 6b displays the length distribution profiles as a function of surface area at 273 K. At this low temperature, the low-density (45 Å^2 molecule^{-1}) system still continues to display a significant degree of structural disorder with a broad distribution of lengths ranging from ∼19.5 to 22 Å^2 molecule^{-1}. However, there is now clearly a peak at 21.7 Å, indicating a significant population of fully extended chains during the simulation. As noted for the 298 K system, the system rapidly moves to an ordered structure with largely elongated chains as the system is compressed. In comparison, there is significantly greater disorder in the system at 368 K, as displayed in Figure 6c. Under low surface density conditions, we observe only a broad, low-intensity distribution ranging from ∼14 to 22 Å with a maximum at ∼19 Å. With compression, the system slowly evolves to greater order until at a surface density of 19.0 Å^2 molecule^{-1}, the length distribution indicates significant order, with only minor contributions from gauche torsions within the alkyl chains.

Figure 7a displays the carbon−carbon RDFs as a function of surface density at 273 K. At low surface density, we observe a similar broad distribution, as noted for the 298 K system. However, as the system is compressed, we observe a more pronounced shift to a two-peak distribution than was observed at 298 K (Figure 2c), reflecting increased order/packing in this more condensed state. Consequently, there should be a significant increase in the energy required to separate the methylene groups of the chains ($\Delta H^{\neq}_{CH_2}$), which should lead to an increase in the evaporation resistance. However, this should be partly offset by an increase in the activation entropy ($\Delta S^{\neq}_{CH_2}$). In contrast, at 368 K (Figure 7b), there is significant chain mobility reflected in greater disorder in the system and, hence, the broad distributions. These results demonstrate that even in the high

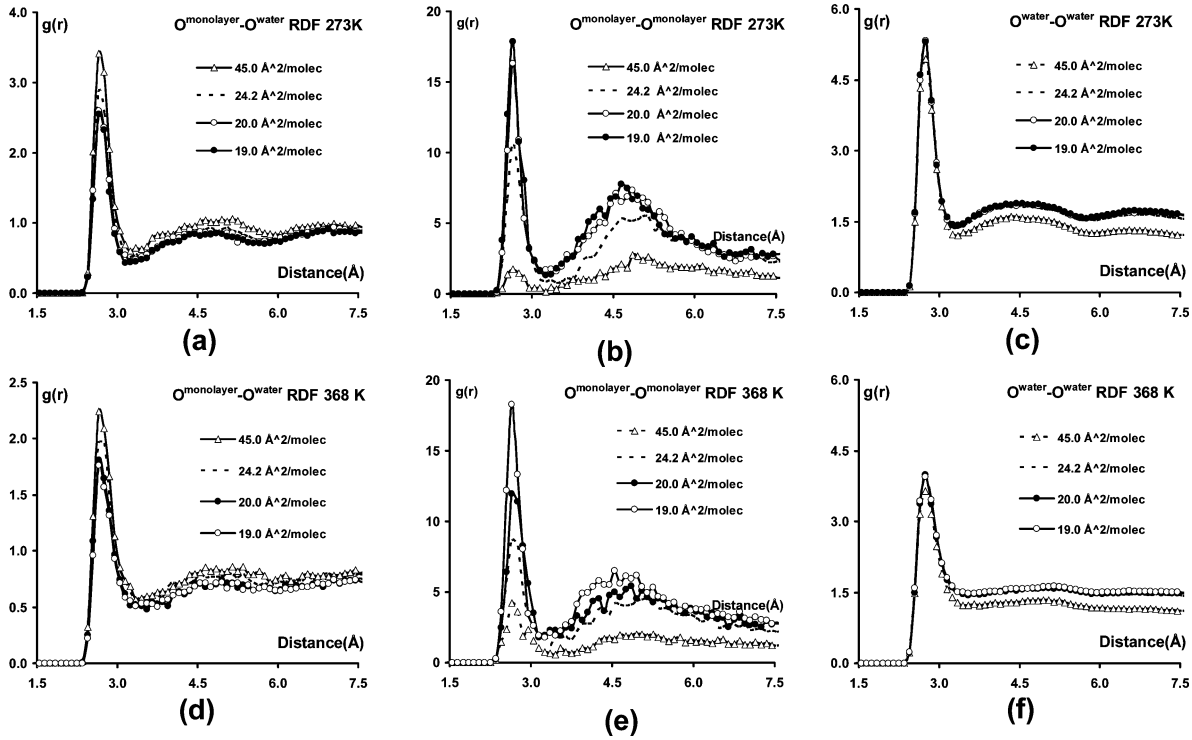

Figure 8. Oxygen−oxygen radial distribution functions (a−c) at 273 K as a function of monolayer surface density and (d−f) at 368 K as a function of monolayer surface density.

surface density region, there is decreased structuring of the chains within the monolayer with increasing temperature. The decreased packing with increasing temperature is reflected in the length distributions and C−C RDFs, which indicate a greater proportion of gauche conformations along the alkyl chains. At high temperature, the alkyl chains are less ordered, so the effective barrier length is smaller and the chains are also spaced farther apart, so there is a weaker interaction between the chains. Therefore, the free energy to separate the chains ($\Delta G^{\neq}_{CH_2}$) should be lower, and hence, this contribution to evaporation resistance will be less. This disorder consequently increases the free volume within the monolayer and therefore increases the number of naturally occurring holes in the monolayer large enough to allow the passage of a water molecule.

Figure 7c displays the free volume within the alkyl region of the monolayer, calculated in terms of H_2O molecules per alkyl chain. The free volume at 273 K is slightly lower than at 298 K for all surface packing densities. At 368 K, there is a greater free volume within the alkyl region, particularly at high surface areas, which agrees with the observed reduction in structuring (Figure 7b). In the experiments of Lo Nostro and Gabrielli,[48] the modulus of compressibility was observed to decrease with temperature and increasing chain length. They observed that longer hydrophobic tails produce stronger interactions between the aliphatic chains and reduce the effects due to the hydrophilic group and its interactions with the subphase. Similarly, they noted that increasing the temperature reduces the compressibility modulus and results in a more expanded monolayer. Our simulations are consistent with the observation that at high temperature, the free volume and, hence, the compressibility within the monolayer is higher, and this also corresponds to the observed trends in evaporation resistance.

Our results are also in agreement with the predictions of the accessible area theory[4] of monolayer permeation, which attributes the major effect of temperature to the expansion of the monolayer with only a relatively minor contribution coming from changes in permeation characteristics. Similarly, the density fluctuation theory[14,15] relates the evaporation resistance to the entropy of expansion of the monolayer and, hence, to the temperature dependence of the surface tension of the substrate.

Figure 8a−c displays the oxygen−oxygen radial distribution functions at 273 K. At low temperature, the $O^{monolayer}$−O^{water} peaks are larger than the corresponding peaks at 298 K and exhibit a slightly larger decrease in intensity between 45.0 and 19.0 Å^2 molecule^{-1}. Similarly, the headgroup−headgroup interactions show a slightly greater increase with surface density, whereas the water−water interactions show essentially no change. At 368 K (Figure 8d−f), the $O^{monolayer}$−O^{water} peaks are slightly smaller than the corresponding peaks at 298 K, but the degree to which the intensity decreases between 45.0 and 19.0 Å^2 molecule^{-1} is quite similar. The headgroup−headgroup interactions ($O^{monolayer}$−$O^{monolayer}$) are also quite similar to those at 298 K and show a steady increase with surface density. Again, the water−water interactions show little change with monolayer surface density. The observation that at low temperature, the headgroup−headgroup interactions show a greater increase in intensity with surface density reflects a more persistent interaction between the OH groups, leading to an increase in the free energy to separate the headgroups ($\Delta G^{\neq}_{h}$) and, consequently, in r (eq 2).

However, at high temperatures, there is relatively little difference from 298 K in the trends for interaction of the headgroups with surface density, suggesting $\Delta G^{\neq}_{h}$ might be less dependent on temperature than $\Delta G^{\neq}_{CH_2}$. Barnes and Quickenden[4] found that if evaporation resistance data was reexamined in terms of constant surface area rather than constant surface pressure, there was a much smaller change in r with T. The apparent temperature dependence of the resistance at constant surface pressure arises from the temperature dependence of the area per molecule. Our observation of the small change in the occurrence of the headgroup−headgroup interactions with

temperature, at constant surface area, is consistent with the findings of Barnes and Quickenden.[4]

4. Conclusions

We have used classical molecular dynamics to probe the principal intermolecular interactions of a monolayer of 1-octadecanol on water to identify factors at the molecular level that contribute to water evaporation suppression. We find good agreement with observations from experimental data available in the literature, where direct comparisons can be made. This demonstrates that our computational methodology, particularly the forcefield, is adequate for this kind of system and provides a reliable foundation for future studies of novel or less characterized systems.

Our simulations demonstrate that at very low surface densities (45.0 Å^2 molecule^{-1}, 298 K) the chains are not fully extended, there is significant disorder, and the alkyl layer thickness is relatively small, therefore providing a relatively small effective barrier for evaporation of water molecules. As the surface density increases, we observe that the alkyl chains generally become fully extended and more ordered, there is less free volume within the monolayer, and the tilt angle of the molecules decreases. At high surface densities, the chains are fully extended, and the tilt angle is relatively small, providing a well-ordered structure that should be an effective barrier to permeation of water.

The trends in the intermolecular interactions can be closely related to features of the current empirical theories of evaporation resistance. Analysis of the alkyl chain structure reveals that the central regions of the chains exhibit the greatest order, followed by the tail region, with the headgroup region exhibiting the greatest disorder. These regions of disorder are significant at low surface densities and, therefore, allow for significant free volume within the chain region, which provides minimal impedance to a permeating water molecule. The carbon−carbon radial distribution functions indicate that next-nearest neighbor interactions are dominant at low surface densities; therefore, the free energy to separate neighboring chains ($\Delta G^{\neq}_{CH_2}$) should be low. However, as the system is compressed, the increased interaction between the carbon chains leads to an increase in $\Delta G^{\neq}_{CH_2}$ and, therefore, in the energy barrier for evaporation. Compression of the monolayer also leads to a significant increase in the interaction between the hydroxy groups of the chains, which results also in a significant increase in the free energy for separation of the headgroups ($\Delta G^{\neq}_{h}$) and, hence, an increased contribution to evaporation resistance. However, at high temperatures, there is relatively little difference from 298 K in the trends for interaction of the headgroups with surface density, suggesting $\Delta G^{\neq}_{h}$ might be less dependent on temperature than $\Delta G^{\neq}_{CH_2}$.

We also identified clear trends in the intermolecular interactions, ordering, and packing of the monolayer molecules as a function of temperature. The average maximum thickness of the monolayer is generally smaller at low temperature, providing a narrow region for water to permeate and, therefore, possibly a reduced barrier length; however, length distributions indicate that the alkyl chains are generally well-extended. The low chain mobility and van der Waals attraction between the chains, is manifested in the more pronounced shift to a two-peak distribution in the carbon−carbon radial distribution function. Consequently, there will be a significant increase in the free energy to separate the methylene groups of the chains ($\Delta G^{\neq}_{CH_2}$) and, hence, an increase in the evaporation resistance, as predicted by the energy barrier theory. Conversely, at high temperature, the alkyl chains are less ordered, so the effective barrier length is smaller, and the chains are also spaced farther apart, so there is a weaker interaction between the chains, and therefore, $\Delta G^{\neq}_{CH_2}$ will be lower, and hence, this contribution to evaporation resistance will be less. At low temperature, the headgroup−headgroup interactions show a greater increase in intensity with surface density, reflecting less disruption to the H-bonding between the OH groups, leading to a greater contribution to $\Delta G^{\neq}_{h}$ and, therefore, r (eq 2).

The increased stability/order between the monolayer chains at lower temperature is also reflected in the lower free volume within the monolayer, and therefore, there is a lower probability (P) of finding holes of adequate size to allow the passage of a water molecule, as described by the density fluctuation theory (eq 5). Naturally, as the temperature is increased, there is greater disorder and more free volume; therefore, P increases, and the evaporation resistance decreases.

Acknowledgment. We gratefully acknowledge the CRC for Polymers for financial assistance and the National Computational Infrastructure (NCI) facility for allocation of computing time. We also thank Dr. Piotr Kowalczyk and Mr. George Yiapanis for helpful discussions.

References and Notes

(1) Rideal, E. K. *J. Phys. Chem.* **1925**, *29*, 1585–1588.
(2) Langmuir, I.; Schaefer, V. J. *J. Franklin Inst.* **1943**, *235*, 119–162.
(3) Archer, R. J.; La Mer, V. K. *J. Phys. Chem.* **1955**, *59*, 200–208.
(4) Barnes, G. T.; Quickenden, T. I.; Saylor, J. E. *J. Colloid Interface Sci.* **1970**, *33*, 236–243.
(5) Barnes, G. T. *J. Hydrology* **1993**, *145*, 165–173.
(6) Craig, I.; Aravinthan, V.; Baillie, C.; Beswick, A.; Barnes, G.; Bradbury, R.; Connell, L.; Coop, P.; Fellows, C.; Fitzmaurice, L.; Foley, J.; Hancock, N.; Lamb, D.; Morrison, P.; Misra, R.; Mossad, R.; Pittaway, P.; Prime, E.; Rees, S.; Schmidt, E.; Solomon, D.; Symes, T.; Turnbull, D. *Environ. Health* **2007**, *7*, 84–97.
(7) Barnes, G. T. *Agric. Water Manage.* **2008**, *95*, 339–353.
(8) Matsumoto, M.; Barnes, G. T. *J. Colloid Interface Sci.* **1992**, *148*, 280–283.
(9) McNamee, C. E.; Barnes, G. T.; Gentle, I. R.; Peng, J. B.; Steitz, R.; Probert, R. *J. Colloid Interface Sci.* **1998**, *207*, 258–263.
(10) Barnes, G. T.; Hunter, D. S. *J. Colloid Interface Sci.* **1990**, *136*, 198–212.
(11) Barnes, G. T. *Colloid Surf., A* **1997**, *126*, 149–158.
(12) Quickenden, T. I.; Barnes, G. T. *J. Colloid Interface Sci.* **1978**, *67*, 415–422.
(13) Barnes, G. T.; La Mer, V. K. In *Retardation of Evaporation by Monolayers: Transport Processes*; La Mer, V. K., Ed.; Academic Press: New York, 1962.
(14) Blank, M. *J. Phys. Chem.* **1964**, *68*, 2793.
(15) Blank, M.; Britten, J. S. *J. Colloid Sci.* **1965**, *20*, 789.
(16) Goodridge, F.; Robb, I. D. *Ind. Eng. Chem. Fundam.* **1965**, *4*, 49–55.
(17) Navon, U.; Fenn, J. B. *AIChE J.* **1971**, *17*, 137–140.
(18) Barnes, G. T.; Feher, A. I. *J. Colloid Interface Sci.* **1980**, *75*, 584–589.
(19) Barnes, G. T.; Hunter, D. S. *J. Colloid Interface Sci.* **1982**, *88*, 437–443.
(20) Seimiya, T.; Sasaki, T. *J. Colloid Interface Sci.* **1966**, *21*, 229–237.
(21) Peng, J. B.; Barnes, G. T. *Thin Solid Films* **1994**, *252*, 44–48.
(22) Harkins, W. D.; Copeland, L. E. *J. Chem. Phys.* **1942**, *10*, 272–286.
(23) Lawrie, G. A.; Barnes, G. T. *J. Colloid Interface Sci.* **1994**, *162*, 36–44.
(24) Copeland, L. E.; Harkins, W. D.; Boyd, G. E. *J. Chem. Phys.* **1942**, *10*, 357–365.
(25) Lautz, C.; Fischer, Th. M.; Kildea, J. *J. Chem. Phys.* **1997**, *106*, 7448–7453.
(26) Bois, A. G. *J. Colloid Interface Sci.* **1985**, *105*, 124–128.
(27) Lautz, C.; Fischer, Th. M. *J. Phys. Chem. B* **1997**, *101*, 8790–8793.
(28) Brezesinski, G.; Kaganer, V. M.; Möhwald, H.; Howes, P. B. *J. Chem. Phys.* **1998**, *108*, 2006–2010.
(29) Lautz, C.; Fischer, Th. M.; Weygand, M.; Lösche, M.; Howes, P. B.; Kjaer, K. *J. Chem. Phys.* **1998**, *108*, 4640–4646.

(30) Steitz, R.; Peng, J. B.; Peterson, I. R.; Gentle, I. R.; Kenn, R. M.; Goldmann, M.; Barnes, G. T. *Langmuir* **1998**, *14*, 7245–7249.
(31) Kaganer, V. M.; Brezesinski, G.; Möhwald, H.; Howes, P. B.; Kjaer, K. *Phys. Rev. E* **1999**, *59*, 2141–2152.
(32) Vollhardt, D.; Emrich, G.; Siegel, S.; Rudert, R. *Langmuir* **2002**, *18*, 6571–6577.
(33) Vysotsky, Y. B.; Bryantsev, V. S.; Fainerman, V. B.; Vollhardt, D.; Miller, R. *Colloids Surf., A* **2002**, *209*, 1–14.
(34) Vysotsky, Y. B.; Bryantsev, V. S.; Vollhardt, D.; Miller, R.; Fainerman, V. B. R. *Colloids Surf., A* **2004**, *239*, 135–140.
(35) Jang, S. S.; Jang, Y. H.; Kim, Y.-H.; Goddard, W. A.; Choi, J. W.; Heath, J. R.; Laursen, B. W.; Flood, A. H.; Stoddart, J. F.; Nørgaard, K.; Bjørnholm, T. *J. Am. Chem. Soc.* **2005**, *127*, 14804–14816.
(36) McMullen, R. L.; Kelty, S. P. *J. Phys. Chem. B* **2007**, *111*, 10849–10852.
(37) Theodorou, D. N.; Suter, U. W. *Macromolecules* **1985**, *18*, 1467.
(38) Meirovitch, H. J. *Macromolecules* **1985**, *18*, 569.
(39) Sun, H. *J. Phys. Chem. B* **1998**, *102*, 7338–7364.
(40) Berendsen, H. J. C.; Postma, J. P. M.; vanGunsterenand, W. F.; Hermans, J. *Intermol. Forces* **1981**, 331–338.
(41) Andersen, H. C. *J. Chem. Phys.* **1980**, *72*, 2384.
(42) Buck, M.; Karplus, M. *J. Phys. Chem. B* **2001**, *105*, 11000–11015.
(43) Our calculated minimum areas are determined from the solidlike *S*-phase region of the octadecanol phase diagram and are therefore slightly smaller than the experimentally determined limit area which arises from the LC phase.
(44) Gericke, A; Simon-Kutscher, J; Hühnerfuss, H. *Langmuir* **1993**, *9*, 3115–3121.
(45) Collazo, N.; Shin, S.; Rice, S. A. *J. Chem. Phys.* **1992**, *96*, 4735–4742.
(46) Ma, G.; Allen, H. C. *Langmuir* **2006**, *22*, 5341–5349.
(47) Schwendel, D.; Hayashi, T.; Dahint, R.; Pertsin, A.; et al. *Langmur* **2003**, *19*, 2284–2293.
(48) Lo Nostro, P.; Gabrielli, G. *Langmuir* **1993**, *9*, 3132–3137.

JP909544A